Beetroot-Mediated Synthesis of ZnO/CdS Nanocomposites: A Study on Their Structural, Morphological, Optical, and Antibacterial Features

Mohammed J. Abdulameer
Mohammed A. Akraa

Department of Physics,
College of Education for
Pure Sciences,
University of Babylon,
Hillah 51002, IRAQ

In this study, ZnO/CdS nanocomposite was obtained via a Co-precipitation method at room temperature using beetroot juice (BRJ). The X-ray diffraction (XRD) results confirmed the formation of the compound, while the field-emission scanning electron microscopy (FE-SEM) revealed semi-spherical particles of approximately 16 nm. Energy-dispersive X-ray spectroscopy (EDX) showed Zn, O, Cd, and S in the composite with respective weight percentages of 64.3%, 32.1%, 2.3%, and 1.4%. The Fourier-transform infrared (FTIR) spectra confirmed Zn-O and Cd-S bonds, supporting successful synthesis. UV-visible spectroscopy revealed strong UV absorbance and an energy bandgap of 3.9 eV. Antibacterial testing demonstrated concentration-dependent inhibition of both *S. aureus* and *E. coli* bacteria. The ZnO/CdS nanocomposite exhibited effective antibacterial activity, particularly at higher concentrations, alongside its optical properties, making it suitable for applications requiring biocompatibility and light absorption.

Keywords: Nanocomposites; Co-precipitation; Antibacterial activity; Beetroot juice
Received: 12 February 2025; **Revised:** 30 March 2025; **Accepted:** 6 April 2025

1. Introduction

Nowadays, in the current era, a significant number of esteemed and esteemed researchers, those who are dedicated to the pursuit of knowledge and wisdom, have become engrossed with a primary focus on the revolutionary and innovative concept known as green synthesis technique [1]. This technique, regarded as a groundbreaking and paramount solution, holds the immense potential to propel humanity into the future, paving the way for cutting-edge technologies and scientific advancements [2]. By harnessing the power of this technique, detrimental and hazardous toxic metals within synthesized materials can be effectively diminished, resulting in a world where the industrial landscape is significantly enhanced [3]. The benefits provided by this groundbreaking method reach across multiple sectors and fields, transforming them in significant ways. The motivating influence from this deep understanding has sparked a fresh determination within the scientific community to further explore eco-friendly materials that exhibit exceptional characteristics [4]. These synthesized materials, endowed with a commendable adherence to environmental principles, exhibit a distinctive and remarkable trait of being poor in adhesion, thereby generating endless possibilities for a multitude of applications [5]. Furthermore, this eclectic assortment of materials boasts a myriad of captivating and diverse morphologies, breathing life into the realm of scientific exploration and discovery [6]. Hydrogen consumers on the entire planet consume our energy equipment significantly per year. Consequently, the indispensable prerequisites of earth resources, equipment lifetime, and molecular stability have given rise to a groundbreaking and innovative roadmap known as the molecular revolution classification, transitioning from the realm of nanotechnology towards the realm of nanocatalyst [7]. The utmost importance of selecting the finest nanocatalyst for any desired reaction cannot be overstated, primarily owing to the colossal demand for its utilization in numerous advantageous applications. These applications entail but are not limited to: the attainment of an exceedingly extensive surface area, the facilitation of ample atoms reactivity, the achievement of efficient electron transfer capabilities, the attainment of thermal or chemical resistance [8]. The thin film zinc oxide/cadmium sulfide nanocomposite (ZnO/CdS-NC) and a few of its named nanocomposites are a completely new potential visible light catalyst. For example, red beetroot (Beta vulgaris) can produce H_2 gas and degrade pollutants by direct mineralization in the environment [9,10]. Due to its significance, zinc oxide has been extensively studied, and various techniques have been developed for its synthesis, including both wet and dry methods, which significantly influence its final properties [11-18]. ZnO has distinctive characteristics, such as a very broad band gap, elevated exciton binding energy at ambient temperature, remarkable electrochemical stability, and anisotropic growth behavior [19]. Furthermore, ZnO is recognized as an environmentally friendly and highly effective absorber of UV radiation [20]. When incorporated in surface coatings such as paints [21] or textiles, ZnO nanostructures demonstrate antibacterial [22], and antifungal [23] activities. Recent photocatalytic evaluations of poly(alkyl siloxane) with

embedded ZnO nanoparticles indicate that this material can serve as a protective coating for sandstone surfaces [24]. To enhance the photocatalytic efficiency of ZnO in the visible spectrum, it is often combined with a photosensitizer [25], facilitating faster charge separation and reducing recombination rates [26]. Cadmium sulfide (CdS), with a bulk band gap of about 2.4 eV and high optical absorption, is particularly suitable as a visible light sensitizer [27,28]. ZnO-CdS composites, in particular, have shown promise in applications such as gas sensing [29], photocatalysis [30-32], water splitting [33], and antibacterial activity [34]. In short, the primary objective of this comprehensive study is to effectively prepare and extensively characterize the remarkable ZnO/CdS nanocomposite. By doing so, we were able to preliminarily confirm how and why sulfur bonds were produced from the red Beetroot extract biopsy report in the spectroscopy analysis results it endeavors to explore and bring to light the tremendous potential of this nanocomposite as an innovative catalyst.

2. Experimental Part

Zinc nitrate hexahydrate $Zn(NO_3)_2.6H_2O$ (MW 297.48) from LOBA Chemie Pvt. Ltd (India) and cadmium nitrate tetrahydrate $Cd(NO_3)_2.4H_2O$ (MW 308.47) supplied by Thomas Baker (Chemicals) Pvt. Ltd. (India) were used to produce the ZnO/CdS nanocomposites, and red BRJ as a Sulfur source. Red BRJ, in contrast to other organic materials such as Thiourea, is abundant and cost-effective. In this research, red BRJ was used as an affordable and straightforward method to produce ZnO/CdS composite. Red Beetroot was thoroughly cleaned, soaked and peeled, and then the juice was extracted and separated to obtain pure and fresh juice.

The ZnO/CdS nanocomposite was synthesized using a co-precipitation method. This entailed amalgamating 200 mL of a solution comprising 1.8 g of zinc nitrate dissolved in 100 mL of deionized water with 18.8 g of cadmium nitrate dissolved in 100 mL of deionized water. Subsequently, 50 mL of red BRJ was incorporated as the sulfur source at ambient temperature. The mixture was permitted to settle for 72 hours, subsequently separated through centrifugation at 4000 rpm for 20 minutes. The precipitate underwent three washes with alcohol and three washes with deionized water, maintaining a consistent centrifugation speed throughout each washing step.

The heat-dried sample was analyzed for surface morphology and elemental composition using FE-SEM (Nawah Sciences Ltd. Co.). The XRD method with Cu Kα radiation (λ = 1.54183 Å) was used to examine the crystallographic characteristics structurally. The XRD was conducted using a Bruker D8 Discover diffractometer in 2θ mode at 45 kV and 40 mA. The sample's surface morphology was analyzed using the FE-SEM method with a HITACHI Model TM3030Plus (ExB Electronics Soft Imaging System) running at 15 kV. The sample's chemical composition was analyzed using EDX (Axia Chemi SEM-Thermo Scientific) in conjunction with the SEM equipment.

This research delves into a groundbreaking and highly innovative new method that completely revolutionizes the synthesis of ZnO/CdS nanocomposites. The key to this remarkable breakthrough lies in harnessing the astounding capabilities of red BRJ [35]. BRJ, scientifically known as Beta vulgaris, is an extraordinary plant that belongs to the Chenopodiaceae family. What makes it truly exceptional is its remarkable repertoire of inorganic and organic compounds, including essential vitamins [36]. However, the true highlight is the presence of an extraordinary compound known as betalain, which is composed of two hydroxylated aromatic rings. This compound showcases unparalleled antioxidant power, making it all the more intriguing [37]. It is this unique mechanism that sets Beetroot apart from other plant juice. But that's not all – the red BRJ also exhibits remarkable prowess in terms of both reduction capabilities and stabilization properties. This further emphasizes the extract's undeniable prowess and incredible potential in advancing nanocomposite synthesis methodologies [38]. This study paves the way for new avenues for future advancements and paves the way for more sustainable and eco-conscious methodologies within the field of nanotechnology [39].

This research discusses the development of a new method of synthesizing nanocomposite ZnO/CdS using red Beetroot pericarp juice. BRJ is a source of sulfur, and CdS and ZnO are metal sulfide and heavy metal oxide particles surrounded by carbon [40]. The pericarp contains betalain, an inorganic compound with high antioxidant capacity as well as known reducing and stabilizing properties. Based on these properties, it can be used in a system containing Cd and Zn ions [41].

This work evaluated structural, morphological, and optical features using several characterisation methods, including XRD for crystallinity, FE-SEM for morphology, and UV-visible spectroscopy for optical properties.

The antibacterial efficacy of the ZnO/CdS nanocomposites was assessed by the agar well diffusion technique against Gram-negative and Gram-positive bacterial strains [42,43]. We aseptically transferred roughly 20 mL of Mueller-Hinton agar from sterile Petri plates and retrieved bacterial strains using sterile wire loops from their original cultures [44]. After inoculating the bacterial cultures, wells of 6 mm in diameter were formed on the agar plates using a sterile tip. Different concentrations of ZnO/CdS nanocomposites were injected into these wells. The inoculated plates with ZnO/CdS NCs and bacterial strains were incubated at 37°C overnight, followed by the measurement and recording of the average diameter of the inhibitory zones [45].

The antibacterial behavior of ZnO/CdS nanocomposites is influenced by their band gap values, which determine the energy required for electron-hole pair generation upon light absorption [46]. Both ZnO and CdS are photocatalytic materials, and their band gaps are crucial for effective charge separation and reactive oxygen species (ROS) production during photocatalysis. ROS play a significant role in antibacterial activity by damaging bacterial cell membranes and proteins [47,48]. An optimal band gap facilitates efficient light absorption while minimizing the recombination of charge carriers. If the band gap is too wide, it limits visible light absorption, while a too narrow gap increases recombination [49].

The ZnO/CdS nanocomposite's band gap (3.9eV) is aligned with the solar spectrum for efficient photocatalysis. CdS enhances visible light absorption, complementing ZnO UV absorption. The combined band gaps of ZnO and CdS determine their overall photocatalytic performance [50]. Photocatalysts kill bacteria through ROS production by absorbing light of a specific wavelength, Promoting electrons to the conduction band from the valence band. For effective photocatalysis, these excited electrons must be separated from the holes to prevent recombination [51]. Separated electrons and holes interact with water molecules on the photocatalyst surface, generating hydroxyl radicals (OH•) through two main pathways: interaction of electrons in the conduction band with water molecules, and interaction of holes in the valence band with water or adsorbed hydroxide ions [52,53] The generated OH• radicals, being non-selective oxidants, target bacterial cell membranes composed of phospholipid bilayers, attacking the double bonds in fatty acid tails and disrupting membrane integrity. This disruption leads to leakage of cellular contents and loss of cellular homeostasis, ultimately killing the bacteria [54].

3. Results and Discussion

The crystalline structure of the sample was analyzed using XRD, which validated the semi-crystalline nature of the nanocomposite, as seen in Fig. (1). The XRD patterns of ZnO/CdS composites display mixed diffraction peaks exclusively from ZnO and CdS and table (1) includes the results obtained from the XRD patterns. Though the characteristic peaks of orthorhombic CdS at 2θ = 19.95°, 20.91°, 23.11°, 24.98°, 32.07°, 33.12°, 36.98°, 39.98°, 44.11°, 51.19°, 55.33°, and 64.12°, corresponding to Miller indices of (110), (020), (111), (021), (112), (002), (130), (220), (040), (042), (042), and (134) peaks of CdS, respectively, are in good agreement with JCPDS 00-015-0086.

ZnO peaks appeared at 2θ = 30.82, 38.45, 46.87, 61.77, and 65.82, corresponding to Miller indices of (100), (002), (102), (103), and (112), respectively, and peaks of hexagonal Zincite ZnO agree with JCPDS 01-075-1533. The average particle size was calculated using the Debye-Scherrer equation as [55]

$$D = k\lambda/\beta\cos\theta \quad (1)$$

where D is the crystallite size, k is the shape factor equal to 0.9, θ is the diffraction angle at maximum peak intensity, β is the full-width at half maximum (FWHM) of the diffraction peak in radians, and λ is the x-ray wavelength

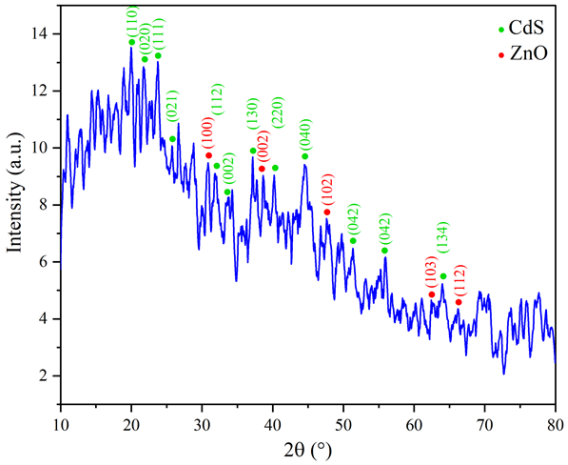

Fig. (1) XRD patterns of the ZnO/CdS nanocomposite

Table (1) The obtained results of the XRD of ZnO/CdS NCs (matched to CdS: 00-015-0086, and ZnO: 01-075-1533)

2θ (deg.)	hkl	FWHM (deg.)	D (nm)
19.95	110	1.378	5.848
20.91	020	0.411	19.611
23.11	111	0.191	42.412
24.98	021	0.662	12.277
30.82	100	0.219	37.534
32.07	112	0.196	41.998
33.12	002	0.09	92.054
36.98	130	0.239	34.905
38.45	002	0.196	42.839
39.98	220	0.103	81.701
44.11	040	0.498	17.194
46.87	102	0.166	51.947
51.19	042	0.09	97.839
55.33	042	0.09	99.629
61.77	103	0.09	102.819
64.12	134	0.09	104.116
65.82	112	0.09	105.105
Mean Crystalline Size			58.225

As shown in Fig. (2), FE-SEM images revealed that the synthesized compound consists of spherical particles, with ImageJ measurements indicating an average particle size of approximately 16 nm. The discrepancy between the nanoscale size obtained from Scherrer's equation and ImageJ arises from the differing calculation methods. Scherrer's equation estimates the size relying on the broadening of XRD peaks, which reflects the dimensions of individual crystals. In contrast, ImageJ measures the actual visible dimensions of the particles using microscopic images, such as SEM or TEM.

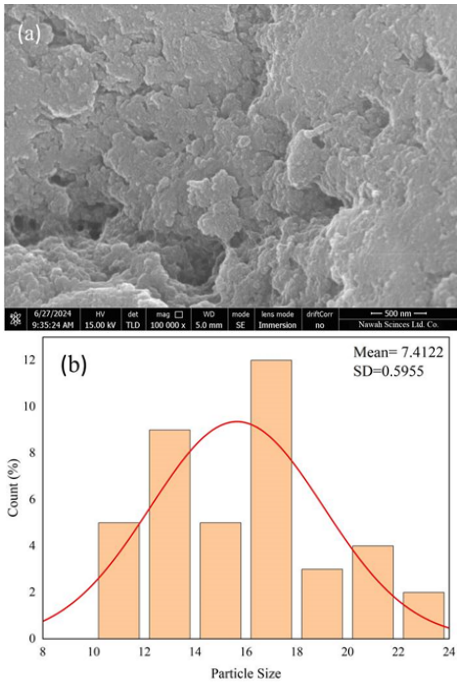

Fig. (2) (a) FE-SEM image of ZnO/CdS nanocomposite and (b) particle size distribution fitted with a log normal distribution function

The EDX spectrum provided offers key insights into the elemental composition of the synthesized material. From the table accompanying the spectrum, we can observe the presence of oxygen (O), sulfur (S), zinc (Zn), and cadmium (Cd). Oxygen emerges as the dominant element, with an atomic percentage of 91.7% and a weight percentage of 64.3%, strongly indicating the presence of oxide compounds, likely ZnO.

The detection of sulfur, albeit in smaller quantities (1.0% atomic and 1.4% weight), suggests the formation of CdS, which is consistent with the expected composition. Zinc is present at 0.8% atomic and 2.3% by weight, reinforcing its involvement in forming ZnO. Meanwhile, cadmium stands out with a higher atomic percentage of 6.5% and a weight percentage of 32.1%, signifying its significant presence in the material, likely as CdS.

The EDX spectrum reveals distinct peaks corresponding to the detected elements. The prominent oxygen peak reflects its abundance in the sample, while the zinc peaks (Zn) are less intense, matching its relatively lower concentration. Cadmium's peaks (Cd) are sharp and strong, indicating its substantial presence, and sulfur's weaker peak aligns with its smaller percentage in the composition. These peaks confirm the expected elemental makeup and indicate the presence of the desired compounds.

The elemental mapping further supports the spectrum's findings. The FE-SEM image (b) highlights a heterogeneous surface morphology. The oxygen map (c) shows a uniform distribution across the sample, reflecting the predominance of oxygen-containing compounds. The zinc map (d) reveals localized regions where zinc is present, suggesting that ZnO is not homogeneously distributed. Cadmium's map (e) shows a broader distribution, though it is still uneven, while sulfur's map (f) indicates sparse areas of sulfur presence, consistent with its relatively low atomic and weight percentages.

The EDX analysis and elemental mapping confirm that the material primarily consists of oxygen, with significant amounts of cadmium, and smaller amounts of zinc and sulfur. This supports the successful synthesis of ZnO/CdS nanocomposites. The higher proportion of cadmium relative to zinc and sulfur implies that CdS may play a more dominant role in the material, making the composite suitable for various applications, such as antibacterial agents or in solar cells, where both ZnO and CdS offer synergistic properties.

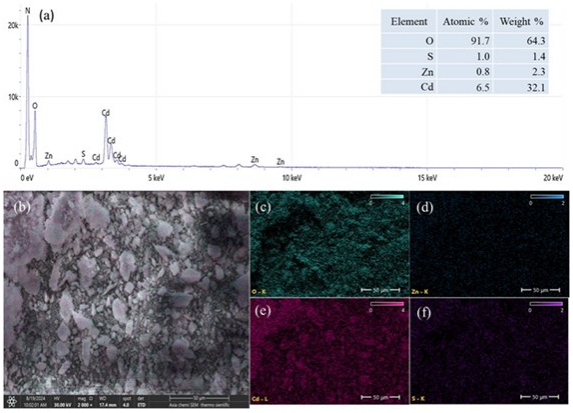

Fig. (3) (a) The EDX spectrum and corresponding elemental mapping (b) ZnO/CdS (c) O, (d) S, (e) Cd, and (f) Zn

In comparison between the FTIR spectra of red Beetroot extract and the nanocompound ZnO/CdS, we observe a range of important changes that indicate the interactions that occur during the preparation process. The FTIR analysis of red Beetroot extract reveals distinctive peaks corresponding to organic compounds, while the spectrum of ZnO/CdS. This signifies the existence of interactions between the juice and the nanocompound, resulting in the emergence of new peaks and the disappearance or change of some peaks in the extract spectrum. A broad peak at 3464 cm^{-1} in BRJ, attributed to O-H vibrations (water or hydroxylic groups), shifts to 3278 cm^{-1} in the ZnO/CdS spectrum. This shift suggests that some O-H groups remain but interact with the surface of the nanomaterial, or it may be due to partial moisture loss during preparation. Furthermore, the disappearance of peak at 2100 cm^{-1} in the ZnO/CdS spectrum, associated with triple bonds (C≡C) in the BRJ spectrum, indicates that these bonds interacted during the preparation process, leading to their breakdown or decomposition.

The peak at 1640 cm^{-1} in the Beetroot spectrum, corresponding to C=C vibrations usually associated

with alkenes, shifts slightly to 1636 cm^{-1} in the ZnO/CdS spectrum. This indicates the involvement of the C=C group in the reaction, although it does not disappear completely, suggesting the survival of some of these organic groups. Additionally, changes in peaks at 1404 and 1057 cm^{-1} in the Beetroot spectrum, which reflect the vibrations of N=O bending (typical of primary or secondary amines) and C-O bonds (linked to carbohydrates and organic compounds), lead to the emergence of new peaks at 1514 and 1365 cm^{-1} in the ZnO/CdS spectrum. This transformation indicates the interaction of organic groups with the nanocompound and the formation of new bonds, possibly between CdS or ZnO and organic compounds.

Moreover, new peaks at 410 and 702 cm^{-1} appear in the ZnO/CdS spectrum, which are absent in the Beetroot spectrum. These peaks are characteristic of nanocompounds and indicate the vibrations of Zn-O and Cd-S, confirming the successful formation of the ZnO/CdS nanocompound. The disappearance or change in peaks related to C≡C, C=O, and O-H groups indicates that these organic groups interacted with other substances during preparation, leading to changes in their chemical structure or their consumption in the reaction. Additionally, the new appearance of peaks associated with Zn-O and Cd-S in the ZnO/CdS spectrum confirms the formation of nano-linkages between zinc and oxygen and between cadmium and sulfur. This suggests that BRJ was an effective source of sulfur in the formation of the nanocomplex [56].

The FTIR spectral analysis demonstrates that BRJ directly contributed to a chemical reaction that resulted in the formation of the ZnO/CdS nanocomplex, serving as a source of sulfur and potentially acting as a stabilizer for the compound.

The UV-visible absorption spectrum, the variation of absorption coefficient, and determination of energy band gap of the prepared Zno/CdS nanocomposite are shown in Fig. (5). The ZnO/CdS nanocomposite exhibits a rapid decrease in absorbance beyond 400 nm, and this demonstrates significant absorption in the UV region along with a reduction in the visible range. This absorption behavior suggests the presence of a direct electronic transition and confirms the nanoscale nature of the material. The observed high absorbance in the UV range aligns with the expected optical behavior of ZnO and CdS components, which are known for their high UV absorbance.

Figure (5b) shows the absorption coefficient (α) plotted against photon energy (eV) [57] where

$$\alpha=2.303A/t \quad (2)$$

where A is the absorbance and t is the optical path length (cm)

The sharp increase in α with increasing photon energy indicates a significant light-matter interaction and suggests the existence of allowed direct transitions within the material. A steep rise in the absorption coefficient at higher energy levels implies that the ZnO/CdS nanocomposite can efficiently absorb photons of certain energies, thereby reinforcing the material's suitability for optoelectronic applications, such as UV detectors and photocatalysis.

Figure (5c) depicts Tauc plot, which plots $(\alpha h\nu)^{1/2}$ against photon energy (hν) to determine the energy band gap of the prepared composite material as [58]

$$\alpha h\nu \approx (h\nu - E_g)^{1/2} \quad (3)$$

Extrapolating the linear region to intercept the energy axis yields the optical band gap value. In this case, the intersection point indicates an estimated indirect bandgap energy of approximately 3.9 eV. This relatively wide bandgap is consistent with the properties of ZnO and CdS semiconductors, emphasizing the composite's potential for applications in fields requiring high-energy photon absorption, such as UV shielding and antibacterial treatments.

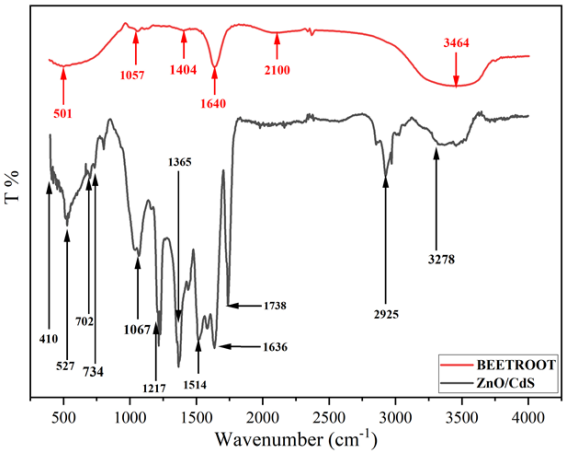

Fig. (4) FTIR spectrum of BRJ and ZnO/CdS nanocomposite

These findings collectively underscore the effectiveness of the synthesized ZnO/CdS nanocomposite in absorbing UV light and its potential applicability in optoelectronics, energy conversion, and photodegradation of pollutants. Furthermore, the wide bandgap energy suggests that the material could exhibit a higher electron-hole recombination threshold, which is desirable for enhanced photocatalytic efficiency.

The antibacterial properties of ZnO/CdS nanoparticles were assessed against various extensively drug-resistant (XDR) bacterial strains *E. coli* (Gram-negative) and *S. aureus* (Gram-positive) using the agar diffusion method. The findings demonstrated that all tested bacterial isolates exhibited sensitivity to the nanoparticles at different concentrations (62, 125, 250 and 500 µg/mL). Notably, the largest inhibition zone observed was 24 mm at the highest concentration of 500 µg/mL, while the smallest inhibition zone, measuring 17 mm, was recorded against *S. aureus* at the lowest concentration of 62 µg/mL. The results indicated a direct correlation between increased nanoparticle concentration and enhanced antibacterial efficacy. These outcomes, as shown in Fig. (6a,b).

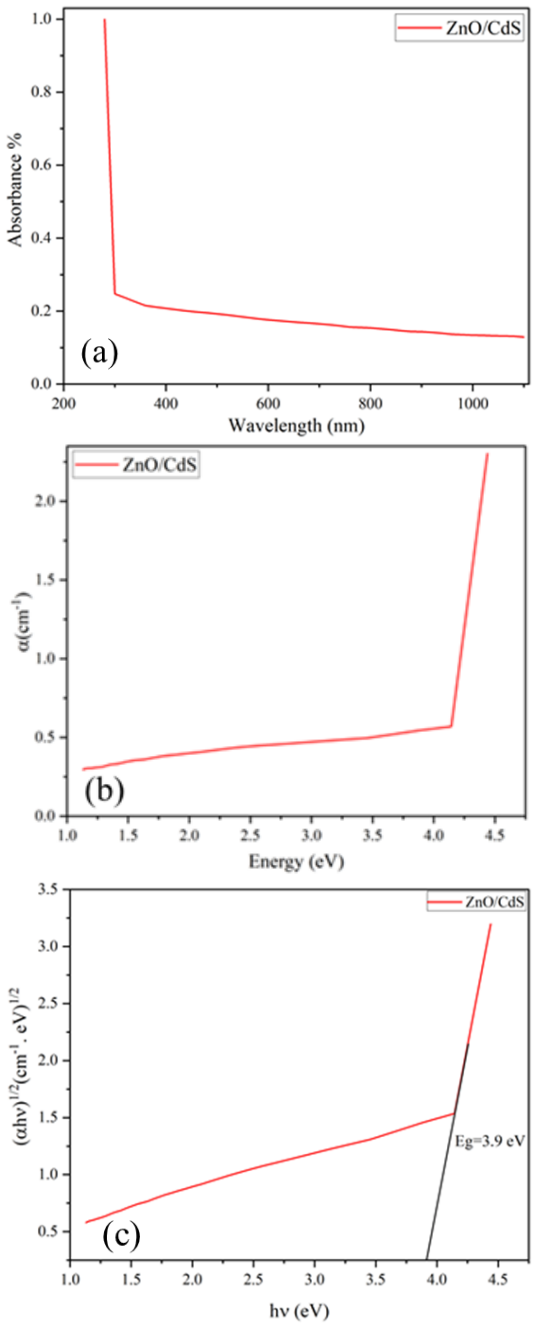

Fig. (5) (a) Absorption spectrum, (b) absorption coefficient, and (c) determination of indirect band gap as functions of photoenergy (*hν*)

To confirm the importance and feasibility of fabricating this nanocomposite using BRJ, we compared its antibacterial efficacy with the ZnO/CdS nanocomposite that we previously fabricated using conventional compounds and reported, including its structural and optical properties [59]. Both nanocomposites were tested for antibacterial activity under identical conditions, using the same concentrations and bacterial strains, to ensure a reliable and consistent comparison as shown in Fig. (7). Using the agar diffusion technique, the antibacterial activity of both materials against *S. aureus* and *E. coli* was evaluated at various doses (62, 125, 250, and 500 µg/mL), as shown in table (2), in the same manner and under the same conditions for each compound separately.

The antibacterial efficacy of ZnO/CdS nanocomposites, as shown by BRJ, exhibited significant variations when evaluated against *E. coli* and *S. aureus*. The ZnO/CdS nanocomposite produced using BRJ exhibited superior antibacterial efficacy against *E. coli* compared to traditional ZnO/CdS at all evaluated doses. The most extensive inhibitory zone was seen at a dose of 500 µg/mL, increasing from 22 mm for conventional ZnO/CdS to 24 mm for ZnO/CdS using BRJ. Conversely, against *S. aureus*, conventional ZnO/CdS exhibited superior antibacterial activity compared to the BRJ-based nanocomposite. At 500 µg/mL, the inhibition zone decreased from 26 mm for conventional ZnO/CdS to 24 mm for ZnO/CdS using BRJ.

These findings suggest that the natural components of BRJ may enhance the antibacterial properties of the ZnO/CdS nanocomposite against Gram-negative bacteria such as *E. coli*, while slightly reducing its effectiveness against Gram-positive bacteria like *S. aureus*. The reduced activity against Gram-positive strains may be attributed to alterations in the surface properties or chemical composition of the nanocomposite resulting from the incorporation of BRJ. Despite this, the enhanced activity against Gram-negative bacteria is a significant advantage, particularly in the fight against antibiotic-resistant strains.

These results underscore the potential of using natural sources, such as BRJ, to improve the antibacterial properties of nanomaterials in a targeted manner. The study highlights the importance of environmentally friendly nanocomposites with tailored antibacterial effects, emphasizing the need to understand differential impacts on various bacterial strains. The GraphPad Prism software was used to statistically analyze the data [58]. These findings are shown as the mean ± SD of the three studies, where a difference of $p<0.05$ is considered statistically significant [60].

Table (2) Antibacterial activity of ZnO/CdS and ZnO/CdS using BRJ against *E. coli* and *S. aureus*

It.	Concentrations (µg/mL)	*E. coli*		*S. aureus*	
		ZnO/CdS	ZnO/CdS using BRJ	ZnO/CdS	ZnO/CdS using BRJ
1	500	22	24	26	24
2	250	20	22	24	22
3	125	17	20	21	18
4	62	15	18	19	17
5	0	6	6	6	6

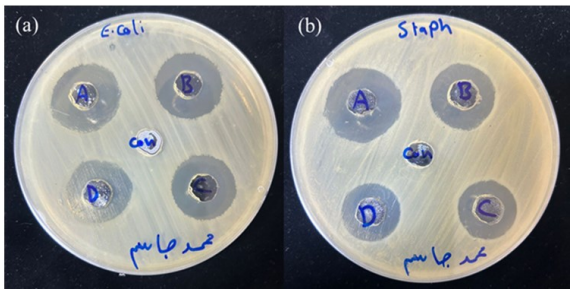

Fig. (6) Antibacterial activity of ZnO/CdS using BRJ against (a) *E. coli*, and (b) *S. aureus*, (A) 500 µg/mL, (B) 250 µg/mL, (C) 125 µg/mL, and (D) 62 µg/mL and control

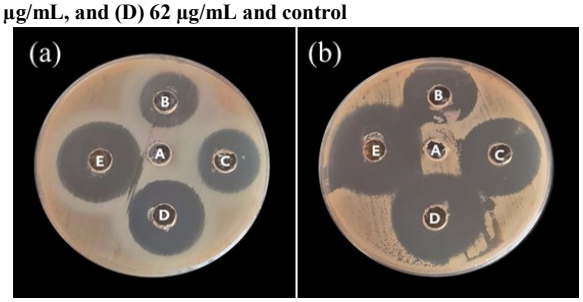

Fig. (7) Antibacterial activity of ZnO/CdS against (a) *E. coli,* and (b) *S. aureus*, (A) control, (B) 62 µg/mL, (C) 125 µg/mL, (D) 250 µg/mL, and (E) 500 µg/mL

4. Conclusions

This study successfully synthesized ZnO/CdS nanocomposites using BRJ, with structural and spectral analyses confirming their purity and uniform nanoscale morphology. Results indicated an average grain size of 16 nm, emphasizing their suitability for optical and antibacterial applications. An indirect band gap of 3.9 eV was revealed making these nanocomposites promising for optoelectronic applications. In terms of biological activity, the material demonstrated antibacterial properties that improved with increasing concentration, suggesting its potential for medical and antimicrobial applications. Compared to conventional materials, this research highlights the benefits of eco-friendly ZnO/CdS synthesis for biomedical and environmental applications. Further studies are recommended to optimize the composition and explore the influence of environmental factors on its properties.

References

[1] H. Abu El-Fotoh, L. Abd El-Rahman, and S. El-Kalawy, "Effect of Sulphur Application and some Foliar Feeding on Productivity and Roots Quality of Sugar Beet", *J. Soil Sci. Agric. Eng.*, 11(11) (2020) 631–639.

[2] M. Thiruvengadam et al., "A comprehensive review of beetroot (Beta vulgaris L.) bioactive components in the food and pharmaceutical industries", *Critic. Rev. Food Sci. Nutr.*, 64(3) (2024) 708–739.

[3] K.M. Elattar et al., "Phytogenic Synthesis and Characterization of Silver Metallic/Bimetallic Nanoparticles Using Beta vulgaris L. Extract and Assessments of Their Potential Biological Activities", *Appl. Sci.*, 13(18) (2023) 10110.

[4] Z. Guo et al., "Active-intelligent film based on pectin from watermelon peel containing beetroot extract to monitor the freshness of packaged chilled beef", *Food Hydrocoll.*, 119 (2021) 106751.

[5] N.B. Singh et al., "Green Synthesis and Applications of Nanomaterials", *Curr. Pharm. Biotechnol.*, 22(13) (2021) 1705-1747.

[6] R.S. Shaikh, R.B. Rajput and R.B. Kale, "Inexpensive green synthesis of natural dye-sensitized solar cells with aqueous solution as a Bi2S3 counter electrode", *Next Mater.*, 3 (2024) 100051.

[7] R. Abedi-Firoozjah et al., "Betalains as promising natural colorants in smart/active food packaging", *Food Chem.*, 424 (2023) 136408.

[8] C. Ungureanu, I. Fierascu, and R. C. Fierascu, "Sustainable Use of Cruciferous Wastes in Nanotechnological Applications", *mdpi Coatings*, 12(6) (2022) 769.

[9] A.R. Amin et al., "Comparison Among Garlic, Berberine, Resveratrol, Hibiscus sabdariffa, Genus Zizyphus, Hesperidin, Red Beetroot, Catha edulis, Portulaca oleracea, and Mulberry Leaves in the Treatment of Hypertension and Type 2 DM: A Comprehensive Review", *Nat. Prod. Commun.*, 15(4) (2020) doi: 10.1177/1934578X20921623.

[10] L.D.S.G. Moreira et al., "Pink pressure: Beetroot (Beta vulgaris rubra) as a possible novel medical therapy for chronic kidney disease", *Nutr. Rev.*, 80(5) (2022) 1041-1061.

[11] N. Preda, M. Enculescu, and I. Enculescu, "Polysaccharide-assisted crystallization of ZnO micro/nanostructures", *Mater. Lett.*, 115 (2014) 256-260.

[12] N. Preda, M. Enculescu, and I. Enculescu, "Polymer sphere array assisted ZnO electroless deposition", *Soft Mater.*, 11(4) (2013) 457-464.

[13] M. Zare et al., "Comprehensive biological assessment and photocatalytic activity of surfactant assisted solvothermal synthesis of ZnO nanogranules", *Mater. Chem. Phys.*, 215 (2018) 148-156.

[14] E. Matei et al., "ZnO morphological, structural and optical properties control by electrodeposition potential sweep rate", *Mater. Chem. Phys.*, 134(2–3) (2012) 988-993.

[15] C. Florica et al., "ZnO nanowires grown directly on zinc foils by thermal oxidation in air: Wetting and water adhesion properties", *Mater. Lett.*, 170 (2016) 156-159.

[16] C. Florica et al., "High performance FETs based on ZnO nanowires synthesized by low cost methods", *Nanotech.*, 27(47) (2016) 475303.

[17] L.V. Podrezova et al., "Comparison between ZnO

nanowires grown by chemical vapor deposition and hydrothermal synthesis", *Appl. Phys. A Mater. Sci. Process.*, 113(3) (2013) 623-632.
[18] L. Frunza et al., "Photocatalytic activity of wool fabrics deposited at low temperature with ZnO or TiO2 nanoparticles: Methylene blue degradation as a test reaction", *Catal. Today*, 306 (2018) 251-259.
[19] S. Khanchandani et al., "Shell thickness dependent photocatalytic properties of ZnO/CdS core-shell nanorods", *J. Phys. Chem. C*, 116(44) (2012) 23653–23662.
[20] H. Wang et al., "*in situ* Synthesis of Flowerlike Lignin/ZnO Composite with Excellent UV-Absorption Properties and Its Application in Polyurethane", *ACS Sustain. Chem. Eng.*, 6(3) (2018) 3696-3705.
[21] S. Sathya et al., "Antibacterial and cytotoxic assessment of poly (methyl methacrylate) based hybrid nanocomposites", *Mater. Sci. Eng. C*, 100 (2019) 886–896.
[22] P. Shubha et al., "Ex-situ fabrication of ZnO nanoparticles coated silk fiber for surgical applications", *Mater. Chem. Phys.*, 231 (2019) 21-26.
[23] F. Zhang et al., "Molecular mechanism and changes of antioxidant enzyme in ZnO nanoparticles against fungus", *J. Biomed. Nanotechnol.*, 15(4) (2019) 647–661.
[24] J. Tokarský et al., "Photoactive and hydrophobic nano-ZnO/poly(alkyl siloxane) coating for the protection of sandstone", *Constr. Build. Mater.*, 199 (2019) 549–559.
[25] J. Nayak, H. Lohani, and T.K. Bera, "Observation of catalytic properties of CdS–ZnO composite nanorods synthesized by aqueous chemical growth technique", *Curr. Appl. Phys.*, 11(1) (2011) 93–97.
[26] H. Zhou et al., "Towards highly efficient photocatalysts using semiconductor nanoarchitectures", *Ener. Enviro. Sci.*, 5(5) (2012) 6732–6743.
[27] O.A. Hammadi and N.E. Naji, "Electrical and spectral characterization of CdS/Si heterojunction prepared by plasma-induced bonding", *Opt. Quantum Electron.*, 48(8) (2016) 375-381.
[28] O.A. Hammadi and N.E. Naji, "Characterization of CdSe/Si Heterostructures Synthesized by Plasma-Induced Bonding Technique", *Iraqi J. Appl. Phys.*, 18(1) (2022) 21-26.
[29] W. Kim, M. Baek, and K. Yong, "Fabrication of ZnO/CdS, ZnO/CdO core/shell nanorod arrays and investigation of their ethanol gas sensing properties", *Sens. Actuat. B: Chem.*, 223 (2016) 599–605.
[30] Y.C. Liang et al., "Microstructure-Dependent Visible-Light Driven Photoactivity of Sputtering-Assisted Synthesis of Sulfide-Based Visible-Light Sensitizer onto ZnO Nanorods", *mdpi Mater.*, 9(12) (2016) 1014.
[31] H. Zhao et al., "Light-Assisted Preparation of a ZnO/CdS Nanocomposite for Enhanced Photocatalytic H_2 Evolution: An Insight into Importance of *in situ* Generated ZnS", *ACS Sustain. Chem. Eng.*, 3(5) (2015) 969–977.
[32] N.M. Jassim, Z.A. Abed and Z.S. Mahdi, "Synthesis, characteristics and study the photoluminscience of the CdS_xSe_{1-x} nanocrystaline thin film", *Baghdad Sci. J.*, 17(1) (2020) 116–119.
[33] S. Cao et al., "Band alignment engineering for improved performance and stability of $ZnFe_2O_4$ modified CdS/ZnO nanostructured photoanode for PEC water splitting", *Nano Energy*, 24 (2016) 25–31.
[34] M. Zirak et al., "Vertically aligned ZnO@CdS nanorod heterostructures for visible light photoinactivation of bacteria", *J. Alloys Compd.*, 590 (2014) 507–513.
[35] A.C.V. de Lima et al., "Microfiltered red–purple pitaya colorant: UPLC-ESI-QTOF-MSE-based metabolic profile and its potential application as a natural food ingredient", *Food Chem.*, 330 (2020) 127222.
[36] A.K. Mall et al., "Sugar Beet Cultivation in India: Prospects for Bio-Ethanol Production and Value-Added Co-Products", *Sugar Tech*., 23(6) (2021) 1218–1234.
[37] S.Z. Asadi and M.A. Khan, "The Effect of Beetroot (Beta vulgaris L.) Leaves Powder on Nutritional, Textural, Sensorial and Antioxidant Properties of Cookies", *J. Culin. Sci. Technol.*, 19(5) (2021) 424–438.
[38] Y. Zhang et al., "Influence of biochar and fulvic acid on the ryegrass-based phytoremediation of sediments contaminated with multiple heavy metals", *J. Environ. Chem. Eng.*, 11(2) (2023) 109446.
[39] H. Salimi Shahraki, A. Ahmad and R. Bushra, "Green carbon dots with multifaceted applications– Waste to wealth strategy", *Flat. Chem.*, 31 (2022) 100310.
[40] V. Popescu, "New trends in the application of natural dyes in textile dyeing", in Renewable Dyes and Pigments, Elsevier (2023) pp. 111-137.
[41] V.N. Zelenkov et al., "Elemental composition of the stems of Beta vulgaris L. var. conditiva Alef. as an indicator of increasing the profitability of functional products", in IOP Conf. Ser.: Earth Enviro. Sci., 650(1) (2021) 12056.
[42] H.H. Bahjat et al., "Magnetic Field-Assisted Laser Ablation of Titanium Dioxide Nanoparticles in Water for Anti-Bacterial Applications", *J. Inorg. Organomet. Polym. Mater.*, 31(9) (2021) 3649–3656.
[43] K.S. Khashan et al., "Anticancer activity and

toxicity of carbon nanoparticles produced by pulsed laser ablation of graphite in water", *Adv. Nat. Sci. Nanosci. Nanotechnol.*, 11(3) (2020) 035010.
[44] K.S. Khashan et al., "Antibacterial activity of Zinc Oxide nanostructured materials synthesis by laser ablation method", *J. Phys. Conf. Ser.*, 1795(1) (2021) 012040.
[45] M.K.A. Mohammed et al., "Functionalization, characterization, and antibacterial activity of single wall and multi wall carbon nanotubes," in *IOP Conf. Ser.: Mater. Sci. Eng.*, 757(1) (2020) 012028.
[46] Y. Xie et al., "Antibacterial activity and mechanism of action of zinc oxide nanoparticles against Campylobacter jejuni", *Appl. Environ. Microbiol.*, 77(7) (2011) 2325–2331.
[47] I. Zgura et al., "Cytotoxicity, antioxidant, antibacterial, and photocatalytic activities of ZnO-CdS powders", *Materials (Basel)*, 13(1) (2020) 182.
[48] A. Salman et al., "Applications of nanotechnology and advancements in smart wearable textiles: An overview", *Egypt. J. Chem.*, 63(6) (2020) 2177–2184.
[49] R.K. Saha et al., "Antibacterial and nonlinear dynamical analysis of flower and hexagon-shaped ZnO microstructures", *Sci. Rep.*, 10(1) (2020) 1–14.
[50] A.H. Ismail et al., "Nano-synthesis, spectroscopic characterisation and antibacterial activity of some metal complexes derived from Theophylline", *Egypt. J. Chem.*, 63(12) (2020) 4951–4962.
[51] K. Hirota et al., "Preparation of zinc oxide ceramics with a sustainable antibacterial activity under dark conditions", *Ceram. Int.*, 36(2) (2010) 497–506.
[52] L. Zhang et al., "Investigation into the antibacterial behaviour of suspensions of ZnO nanoparticles (ZnO nanofluids)", *J. Nanoparticle Res.*, 9(3) (2007) 479–489.
[53] L. Zhang et al., "ZnO nanofluids-A potential antibacterial agent", *Prog. Nat. Sci.*, 18(8) (2008) 939–944.
[54] J. Pasquet et al., "The contribution of zinc ions to the antimicrobial activity of zinc oxide", *Colloids Surf. A Physicochem. Eng. Asp.*, 457(1) (2014) 263–274.
[55] H.K. Moudgil, **"Text-Book of Physical Chemistry"**, PHI Learning (2010), Ch. 7, p. 261.
[56] P. Larkin and P. Larkin, **"Infrared and Raman Spectroscopy: Principles and Spectral Interpretation"**, Elsevier (2011), Ch. 8, pp. 153-158.
[57] F. Urbach, "The long-wavelength edge of photographic sensitivity and of the electronic absorption of Solids", *Phys. Rev.*, 92(5) (1953) 1324.
[58] J. Tauc, "Optical Properties of Amorphous Semiconductors," in Amorphous and Liquid Semiconductors, Springer (MA, 1974), pp. 159-220.
[59] M.J. Abdulameer and M.A. Akraa, "Synthesis and Analysis of ZnO/CdS Nanocomposites : Structural and Optical Properties", *Iraqi J. Appl. Phys.*, 20(4) (2024) 853–858.
[60] M.L. Swift, "GraphPad prism, data analysis, and scientific graphing", *J. Chem. Inform. Comput. Sci.*, 37(2) (1997) 411–412.

